PHILOSOPHICAL TRANSACTIONS OF THE ROYAL SOCIETY B BIOLOGICAL SCIENCES

Human Whole Body Imaging and Detection of Breast Tumours by n.m.r.

P. Mansfield, P. G. Morris, R. J. Ordidge, I. L. Pykett, V. Bangert and R. E. Coupland

Phil. Trans. R. Soc. Lond. B 1980 **289**, 503-510
doi: 10.1098/rstb.1980.0069

Phil. Trans. R. Soc. Lond. B **289**, 503–510 (1980) [503]
Printed in Great Britain

Human whole body imaging and detection of breast tumours by n.m.r.

By P. Mansfield, P. G. Morris, R. J. Ordidge, I. L. Pykett,
V. Bangert and R. E. Coupland†

Department of Physics, University of Nottingham, University Park, Nottingham NG7 2RD, U.K.
† *Department of Human Morphology, Queen's Medical Centre, University Hospital, Clifton Boulevard, Nottingham NG7 2UH, U.K.*

[Plates 1 and 2]

A brief review of recent developments in line scan imaging of large objects is given, together with some representative images showing anatomical detail and a discussion of some spin–lattice relaxation time mapping results.

Current progress in high speed imaging by means of the echo planar technique is reported and some preliminary results obtained at both 15.0 and 4.0 MHz are discussed.

1. Introduction

Several quite different approaches to the problem of producing spin density images have been reported in the last few years. Most of these methods are discussed and compared by Brunner & Ernst (1979).

A number of small scale images of a live human finger (Mansfield & Maudsley 1976, 1977), a wrist (Hinshaw *et al.* 1977) and various sections through an arm (Hinshaw *et al.* 1979) have been reported. Extensions of imaging apparatus up to whole human body dimensions have also recently been accomplished (Damadian *et al.* 1977; Mansfield *et al.* 1978).

Following a summary of our results with the whole body line scanning apparatus, the object of this paper is to describe current developments in high speed imaging based on the 'echo planar' method (Mansfield & Pykett 1978).

2. Tissue characteristics

Although n.m.r. may be used to study a whole range of magnetic nuclei occurring naturally in biological tissue, for example, ^{31}P and ^{13}C, in our work we have concentrated on the mobile proton resonance of ^{1}H nuclei contained in the water, fat and oil distributed in the tissues and organs. Human tissue contains, on average, about 70% water. Excluding the bulk body fluids, which contain about 95% water, and bone tissue, which contains about 12% water, there is a spread of water content, among the various healthy tissues and organs, of approximately 15%. N.m.r. imaging of anatomical detail is thus feasible based purely on the measurement of water content. There are, however, other important n.m.r. parameters commonly measured in conventional studies. One of these is the spin–lattice relaxation time, T_1, which is also found to be different among the various tissues and organs. Most n.m.r. imaging techniques can be adapted to measure T_1 and a knowledge of this parameter may be of diagnostic value since it has been demonstrated that certain tumours have T_1 values generally longer than those of the surrounding normal tissue (Damadian 1971).

3. Line scanning

One method that we have devised to inspect the spin density distribution, $\rho(xyz)$, and $T_1(xyz)$ is the line scanning technique based on selective irradiation. The method, which has been described in detail elsewhere (Mansfield *et al.* 1976), effectively isolates the n.m.r. free induction decay (f.i.d.) signal emanating from a narrow rectangular column of material within the specimen. The f.i.d. is Fourier transformed to yield the line spin density or an effective density which includes variations in T_1. The spin density data, which form one line of the image, are stored in a computer memory. The line defining process is repeated for successive adjacent columns of material in a plane, and an image of the scanned plane built up line by line. On completion of the scan, the image data are output in the form of a black and white or colour image. If two or more images of the same scan plane are formed with different repetition rates, it is a straightforward matter to separate $\rho(xyz)$ and $T_1(xyz)$. In this instance a pure spin density image may be formed as well as the corresponding T_1 map.

Our first whole body line scan images are, in fact, composite functions of spin density and relaxation time (Mansfield *et al.* 1978).

Figure 1, plate 1, shows a cross-sectional view through the abdomen of P.M. at the L2–L3 level. The slice thickness in this instance is about 4.0 cm and the scan time is 40 min.

The general outline of the cross section is clearly seen, with the anterior aspect upper left. The liver mass shows as a bright zone to the right. The loss of signal at the abdominal wall is attributed to both respiratory motion and a progressive phase change throughout the scan. Other anatomical features, such as the spleen, gall bladder, kidneys, vertebral column and intestinal regions can be distinguished in the picture.

The image data were processed to form the picture with an Optronix photowriter (see acknowledgements) using 256 grey levels on a two cycle display. The darker region in the liver mass corresponds to the second data display cycle, in which black corresponds to signal level 128. The rest of the picture lies within the first display cycle, with an intensity range of 0–127.

The line scanning apparatus has also been used to examine tumorous breasts shortly following mastectomy (Mansfield *et al.* 1979). Figure 2*a*, *b*, plate 1, shows coronal projection scans of the breast, performed at two different scan repetition periods to observe spin–lattice relaxation effects. Figure 2*a*, is a relatively slow scan with a repetition period of 0.3 s. This image shows the general outline of the breast, which had a missing notch of material to the left. The dark region to the right is the nipple. Figure 2*b* shows the same breast scanned at a faster rate, with a repetition period of 0.15 s. The dark central zone in the image corresponds well with the main core of the tumour, a scirrhous carcinoma. Figure 2*c* shows the position and extent of the tumour obtained from serial sections through the breast, histological examination and from reconstruction of the specimen; these sections were made after fixation of the mass in formalin following completion of the n.m.r. scans. The circle shows the position of the nipple. The axillary tail lies to the top of the scans.

The data have also been used to obtain a T_1 map of the breast, representing over 3000 independent T_1 measurements, which we have displayed in colour. Apart from some anomalously high T_1 values at the edge of the map in the axillary tail region, the T_1 map gives quite good spatial correlation and correspondence with the histologically identified regions of the specimen. The anomalies result from mis-registering of the data and also from the poorer

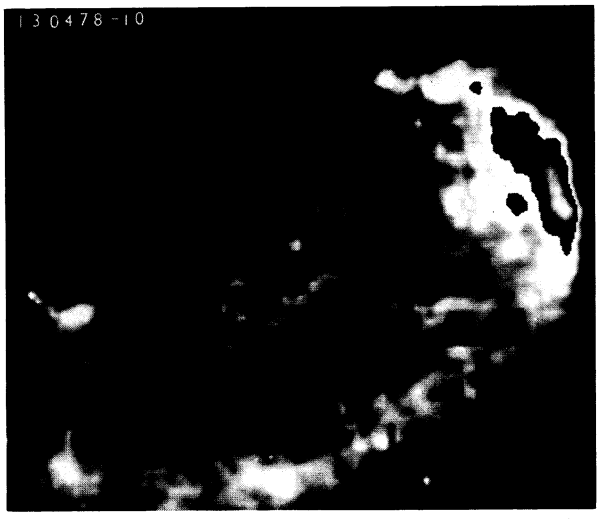

1

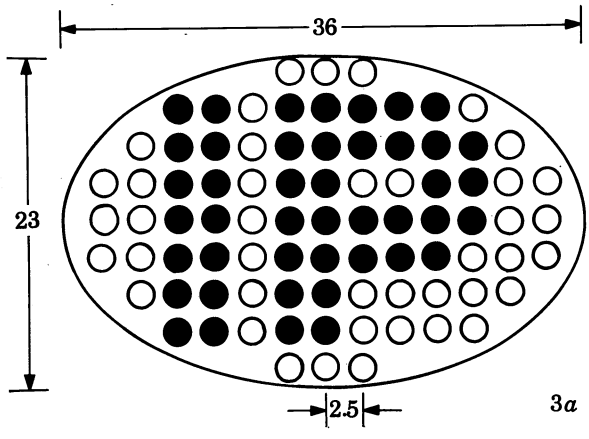

3a

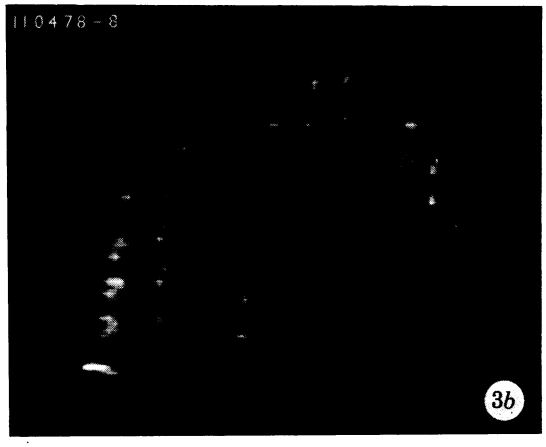

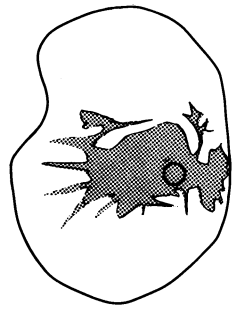

2c

FIGURE 1. Live cross-sectional image through the abdomen of P.M. at the L2–L3 level. Slice thickness is approximately 4.0 cm and the imaging time 40 min. See text and reference for further details.

FIGURE 2. Coronal projection scans through a tumorous breast shortly after mastectomy; (*a*) repetition period 0.3 s; (*b*) repetition period 0.15 s; (*c*) tracing taken from serial sections through the breast after n.m.r. scanning. This sketch shows the general outline of the breast with axillary tail uppermost. The shaded region shows the extent of the tumour which had its greatest depth and mass slightly left of the nipple (circle).

FIGURE 3. (*a*) Sketch of test phantom comprising an ellipical support matrix with an array of 19 mm diameter holes drilled with centres spaced at 25.4 mm intervals. (N.B. Dimensions in the diagram are shown in cm.) The filled circles represent test tubes containing water, forming the letters I P. (*b*) N.m.r. image of the phantom in (*a*) above. The slope and variation in intensity of the letters indicates the distortion of the gradient fields caused by non-uniformity of the main static magnetic field.

(*Facing p.* 504)

PHILOSOPHICAL TRANSACTIONS OF THE ROYAL SOCIETY B BIOLOGICAL SCIENCES

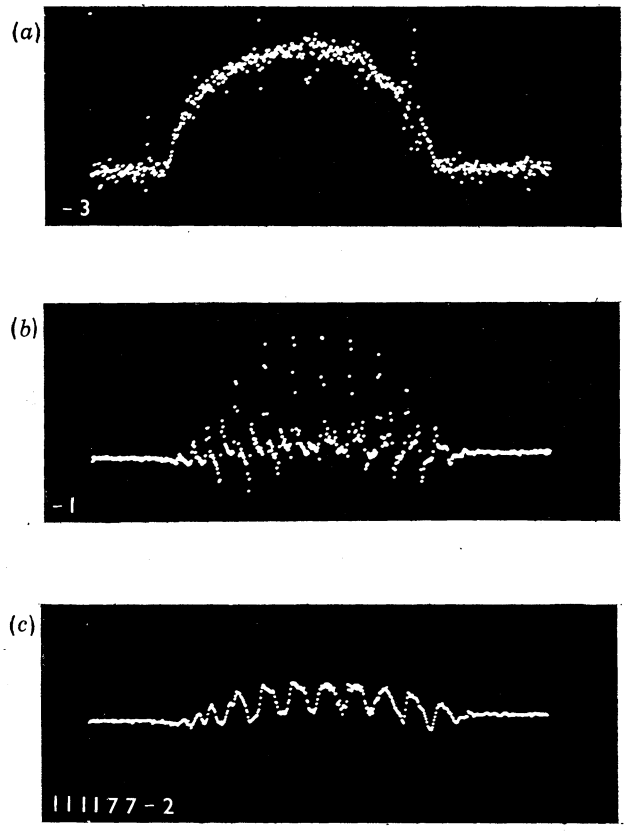

FIGURE 7. Experimental spin projections obtained at 15.0 MHz for a homogeneous cylinder of mineral oil: (*a*) continuous spin projection with steady gradient G_y; (*b*) discrete projection when G_y is modulated; (*c*) broadened discrete projection obtained as in (*b*) above, but with the addition of a steady gradient G_z (see also figure 5).

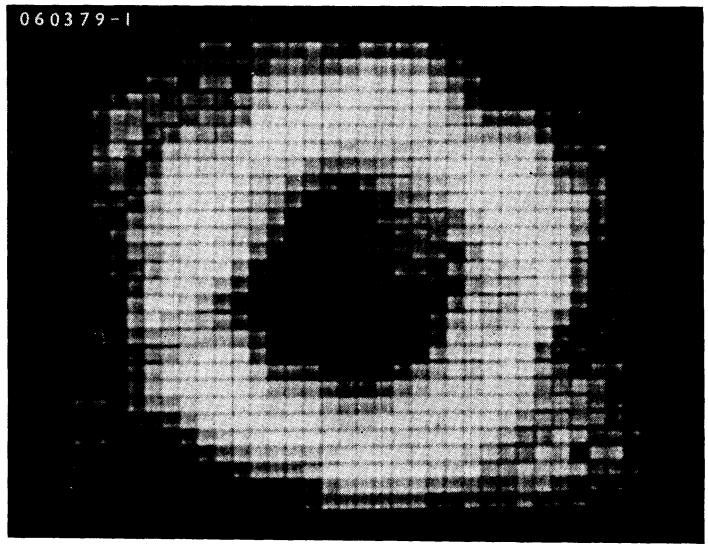

FIGURE 8. Echo planar image of a 1.5–2.0 cm thick selected slice through an extended cylindrical annulus of water, obtained at 4.0 MHz. The total image field is represented by a 32×32 array of original data points. This image was obtained in 8.0 s. The outer diameter of the phantom was 4.8 cm.

PHILOSOPHICAL TRANSACTIONS OF THE ROYAL SOCIETY B BIOLOGICAL SCIENCES

signal/noise ratios in the thinner peripheral regions of the sample. In fact, the specimen thickness tapers off from about 4.0 cm at the centre to about 1.0 cm at the edge.

The main mass of material, which is assumed to be unaffected by the tumour, though we cannot rule out a systemic effect, is characterized by T_1 values in the range 100–370 ms, with a mean value of 164 ms and a standard deviation of ± 90 ms. The tumour core has T_1 values mainly in the range 750–1000 ms, with a single point error of $\pm 35\%$, but there are some high spots that remain undetermined. The core, which is around 25 mm long by 15 mm wide, is surrounded by a well defined contour band of T_1 values in the range 530–750 ms, with a single point error of $\pm 25\%$.

There is also a well defined region of long T_1 values, in the range 750–1000 ms, with a single point error of $\pm 35\%$, surrounding the nipple, out to a radius of about 10 mm, again banded by a thin contour of T_1 values in the range 530–750 ms, extending just to the tumour core region. The central nipple region seems to have T_1 values greater than 1000 ms, but the accuracy of the data here is lower than elsewhere because of the lower water content and poorer signal/noise ratio.

The two high T_1 spots described lie within an intermediate T_1 zone extending over a region of the breast that corresponds rather well with the shaded region of figure 2*c*. The T_1 values in this zone lie in the range 320–530 ms, with a mean of 420 ± 83 ms, and are undoubtedly weighted average values of normal tissue and interpenetrated malignant material.

The procedure used to extract the T_1 values and also the true spin density distribution (not shown here), which assumes a one component spin–lattice relaxation process, will be described elsewhere.

Images of a number of other specimens, including cadaver brains, limbs etc., have been produced. A two-dimensional projection image of a live hand, which we have produced recently, demonstrates the n.m.r. image counterpart of a normal X-ray shadow graph. This type of imaging, though not so detailed, may nevertheless be of value, in studies of the vascular system, for example.

4. Experimental

All line scanning experiments have been performed at a proton resonance frequency of 4.0 MHz. The static magnetic field necessary for these experiments (*ca.* 940 G†) is provided by an Oxford Instruments electromagnet with an overall access of 64.5 cm. Home-built gradient coils and a switching unit produce linear magnetic field gradients, each of magnitude 0.04 G m^{-1}, along the three principal axes. The gradients switch on and off in approximately 50 μs. Selective r.f. pulses of 7.4 ms duration and peak power of 10 W were applied repetitively, every 0.3 s, to give images of live specimens.

To check the extent of image distortions present, a phantom of test tubes containing water was constructed using a supporting grid, as indicated in figure 3*a*, plate 1. The test tubes were 19 mm in diameter and 35 mm long and were arranged in the shape of the letters I P.

The n.m.r. image of this array is shown in figure 3*b* and clearly demonstrates both spatial and intensity distortions. Non-uniformity of the static magnetic field is thought to be largely responsible for the spatial distortions and will contribute to the intensity effects as well. The non-uniformity of the magnetic field is caused primarily by distributed iron in the structure of the present laboratory.

† $1\,G = 10^{-4}\,T$.

5. High speed imaging

The line scanning technique discussed above has been useful in our initial evaluation studies of n.m.r. imaging. It has enabled us to obtain a feel for what is obtainable at low frequencies in terms of morphological detail and spin–lattice relaxation time variations. However, the method is inherently a slow one. Actual scan times achieved vary from 15 to 40 min and depend on selective pulse repetition rate, the degree of signal averaging used and the size of the object relative to a fixed elliptical imaging field of 36×23 cm. The order in which the line scan experiment proceeds makes some difference to the scan time. For example, if data averaging is completed on one picture line before moving to the next line, the signal averaging repetition period cannot be too different from T_1 if image contrast enhancement through relaxation time effects is to be avoided. If, on the other hand, the whole picture is line scanned once, it is not necessary to wait between lines for an interval equal to T_1. The scan speed is really limited by the control hardware and the data handling speed of the apparatus. Of course, to achieve the desired signal:noise ratio, many pictures so produced may be co-added. The time saved by re-ordering the experimental procedure in line scanning experiments could be a factor of up to ten. This would mean that human whole body images could possibly be produced in about 4.0 min.

Although this represents a welcome reduction in scan time, it has to be judged against the inherent time scales caused by involuntary motions in a subject. These may be conveniently divided into three time régimes. The slowest is breathing and under favourable circumstances a subject could be expected to suspend breathing for up to 20 s. The second régime arises from the irregular motions of the stomach and intestines and occurs typically on a time scale of about 3 s. The fastest time régime is, of course, the heart beat, which occurs roughly every 0.8 s. However, in order to image a beating heart it would be necessary to form complete pictures in times less than 100 ms.

It would seem, therefore, that imaging methods based on line scanning principles would have applications limited to those parts of the anatomy where involuntary motion is negligible, for example, the head and limbs. For these reasons, we have been led to consider alternative, and potentially faster, imaging techniques. In one of these methods, which we call 'echo planar imaging' (Mansfield & Pykett 1978), all signals from a selected plane through the specimen are simultaneously received and differentiated. By this means it is possible to form single shot pictures in under 100 ms. Of course, if signal : noise enhancement is required, it is necessary to repeat the imaging process. Nevertheless, the overall imaging times are considerably reduced.

5.1 *Echo planar imaging*

To understand this method of imaging, we consider an object field in the form of a square array of 4×4 small holes into which thin tubes of fluid can be placed, as in our line scan phantom. Figure 4 shows the array partially filled (black dots) to form the letter F. When a gradient, G_x or G_y, is applied along the principal axes, x or y, of the grid, the total spin density projection orthogonal to the gradient direction is obtained, and, from or two such projections, it is, in general, impossible to deduce the details of the object. For an image matrix comprising m^2 elements, one requires, in general, m projections of the object to reconstruct a completely determined image. However, in our case, if the tubes are thin enough and the grid spacing large enough, there is one special field gradient direction, G_s, that reveals the entire internal

structure in a single projection, as shown in figure 4. Thus, if the object were examined in this special gradient, G_s, and the f.i.d. taken and Fourier transformed, all the points of the F would be simultaneously resolved, as shown. It is then a simple matter to order the projection data to form an image of the letter F.

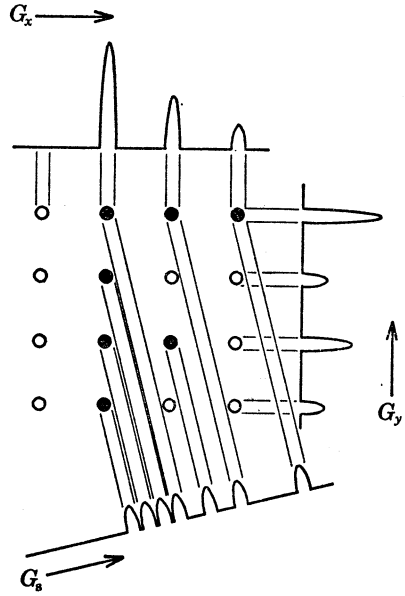

FIGURE 4. Sketch of a discrete letter F with various spin density projections.

The above argument applies only to a discrete spin distribution. There is no special projection axis for a continuous spin distribution. It might therefore appear impossible to apply this imaging principle to continuously distributed spin systems. However, it turns out to be possible to make a continuous spin distribution *appear* discrete. This is achieved by exploiting the refocusing properties of spin echoes, produced in our case by reversing a field gradient, rather than by using a train of 90 ° or 180 ° r.f. pulses. To clarify this we refer to figure 5, which shows the sequence of pulses and gradients used in a three-dimensional echo planar imaging experiment, together with the expected nuclear signal response.

In period A, a slice selection gradient, G_x, is switched on together with a selective r.f. pulse, both for a time t_a. Immediately following the pulse, the f.i.d. signal is observed in a modulated gradient, G_y, of period 4τ, and in á steady, smaller gradient, G_z. The effect of the modulated gradient is to cause the f.i.d. signal to rapidly decay and grow periodically in a series of spin echoes. The effect of G_z is to cause the decay of successive echo peaks over the time period t_b. The trapezoidal gradient waveform of G_y may be replaced by a cosinusoidal form. This type of echo planar imaging will be discussed elsewhere (Mansfield & Ordidge 1980). The sequence is repeated cyclically following a delay t_d.

During the B phase, the entire nuclear signal (including the echoes) is sampled and Fourier transformed. The periodicity in nuclear signal produces a corresponding periodicity in the transformed signal. This is illustrated in figure 6 for the example of an annulus of continuously and uniformly distributed material. The dotted line in figure 6*a* shows the usual continuous projection of an annulus in a steady gradient G_y. The effect of modulating G_y, as in figure 5, is to turn the continuous projection distribution into a discrete form, indicated by the black distribution in figure 6*a*.

PHILOSOPHICAL TRANSACTIONS OF THE ROYAL SOCIETY B BIOLOGICAL SCIENCES

Figure 6*b* shows the annulus, of thickness Δx (previously selected in G_x), and the effective spin distribution present when modulation of G_y is performed. The total spin distribution now behaves as though it were heaped together into a regular grid structure as indicated. Finally, switching on G_z in addition to modulating G_y effectively rotates the annulus slightly so that one can now view the discrete distribution in profile, rather than end on as in figure 6*a*. The

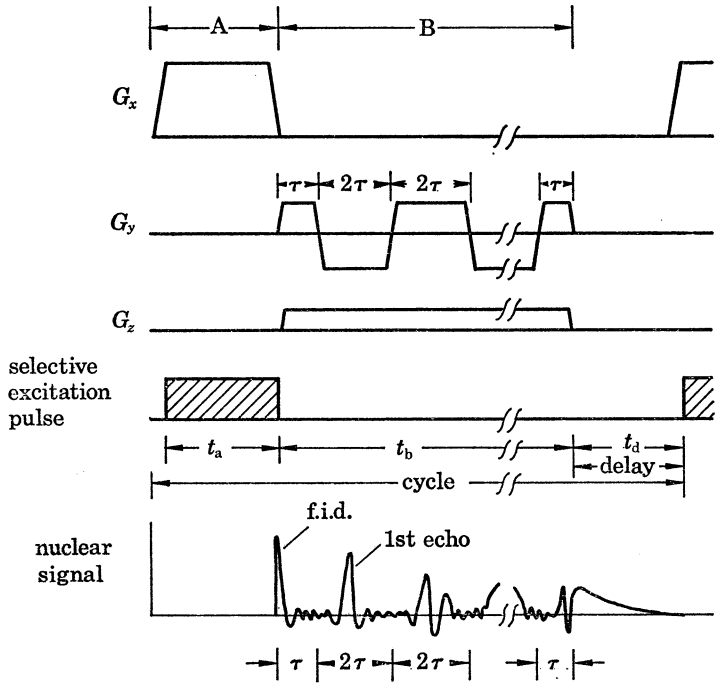

FIGURE 5. Pulse timing sequence used for three-dimensional echo planar imaging experiments.

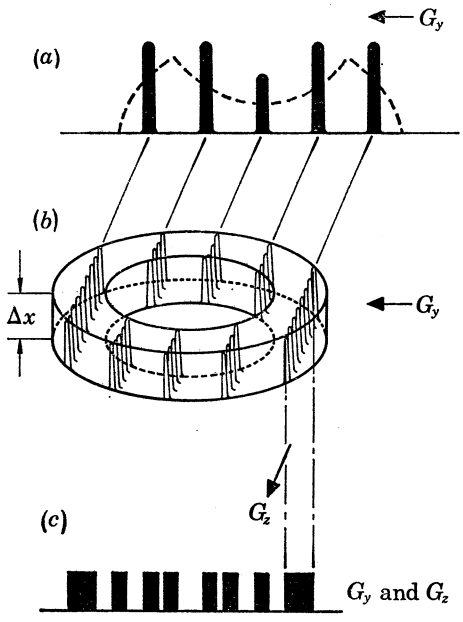

FIGURE 6. Sketch of an annulus of homogeneously distributed spins and the various expected spin projections when subjected to gradient fields as indicated in figure 5.

projected profile is sketched in figure 6*c* and contains sufficient information to deduce the two-dimensional structure.

Figure 7, plate 2, shows some early experimental results obtained with a homogeneous cylinder of mineral oil. The data were obtained at 15.0 MHz with a conventional n.m.r. magnet. The cylinder diameter was 13.8 mm. Figure 7*a* shows the continuous projection profile of the cylinder with a steady value of $G_y = 1.26$ G cm^{-1}. Figure 7*b* shows the effect of modulating G_y as previously described. In this instance, $4\tau = 1.28$ ms and $t_b = 10.24$ ms. Notice the improved signal : noise ratio of the discrete profile over that of the continuous profile. The slight undershoot of signal towards each edge of the profile is caused partly by slight imbalance of the positive and negative amplitudes of G_y. Figure 7*c* shows the discrete profile broadened with the addition of G_z ($= 0.23$ G cm^{-1}), the timing of which is as illustrated in figure 5. In the case of a homogeneous cylinder of spins, successive strips across the cross-sectional disk of material should all have rectangular profiles of constant height, but with varying width. In this example, which corresponds to about nine strips across the cylinder, only the centre three or four are correctly shaped. A contributory factor to the deterioration of profile shapes at the cylinder edges is again the switched gradient amplitude imbalance referred to above.

Because of the mode of operation of echo planar imaging, as we have seen, magnetic field gradients of substantially different magnitudes along at least two orthogonal axes are required to be switched or modulated quite rapidly. The technical problems associated with producing these gradients for a full scale human imaging system could be severe. The problems reduce considerably with size of gradient coil. For this reason we have constructed an approximate one-third scale echo planar imaging system which has an elliptical object field of 10^2 cm $\times$ 7.5 cm. Slice definition through the specimen is again achieved by means of a selective pulse together with a small gradient. Only preliminary results have been obtained with the apparatus with phantoms and a live rat. The slice thickness is about 1.5–2.0 cm and the image field includes 32×32 original data points. Total imaging times vary from 5.0 to 8.0 s, plus Fourier transformation.

An example of an echo planar image produced from a phantom at 4.0 MHz is shown in figure 8. The object in this case is an extended cylindrical annulus of water, of outer and inner diameters 4.8 and 2.5 cm, respectively. The gradient period, 4τ, used was 2.048 ms with 64 sample points per period equally spaced at 32 μs. In this example, the total time to produce a single shot image from a selected slice was $t_b = 65.536$ ms plus 7.4 ms for the initial selective pulse. The image of figure 8, which is an average of 16 separate shots with a delay, t_d, = 0.5 s, took 8 s to produce. The gradient values used were: $G_x \approx 0.02$ G cm^{-1}, $G_y \approx 0.6$ G cm^{-1} and $G_z \approx 0.02$ G cm^{-1}, and the trapezoidal waveform rise and fall times were approximately 25 μs.

Our first images, produced at 4.0 MHz, although somewhat crude by our current line scanning standards, nevertheless indicate the essential features of the object. Some loss in quality is undoubtedly due to the previously mentioned large magnetic inhomogeneities in our static field.

Some picture distortion can also be ascribed to gradient nonlinearities and gradient amplitude imbalance. Improvement in image quality is expected when the present magnet and apparatus are transferred to a recently completed non-magnetic building.

PHILOSOPHICAL TRANSACTIONS OF THE ROYAL SOCIETY B BIOLOGICAL SCIENCES

We are grateful to the Medical Research Council for support of our whole body imaging project and to the Science Research Council for some staff support and for use of the Photowriter facility at the Appleton Laboratory, Slough.

We are particularly indebted to T. Baines for the design and construction of the electronic apparatus and to D. Kerr for the construction of the probe and gradient coil systems.

References (Mansfield *et al.*)

Brunner, P. & Ernst R. R. 1979 *J. magn. Reson.* **33,** 83–106.
Damadian, R 1971 *Science, N.Y.* **171,** 1151–1152.
Damadian, R., Goldsmith, M. & Minkoff, L. 1977 *Physiol. Chem. Phys.* **9**, 97–100.
Hinshaw, W. S., Bottomley, P. A. & Holland G. N. 1977 *Nature, Lond.* **270**, 722–723.
Hinshaw, W. S., Andrew, E. R., Bottomley, P. A., Holland, G. N., Moore, W. S. & Worthington, B. S. 1979 *Br. J. Radiol.* **52**, 36–43.
Mansfield, P., Maudsley, A. A. & Baines, T. 1976 *J. Phys.* E **9**, 271–278.
Mansfield, P. and Maudsley, A. A. 1976 *Proc. 19th Ampere Congress* (*Heidelberg*), pp. 247–252.
Mansfield, P. & Maudsley, A. A. 1977 *Br. J. Radiol.* **50**, 188–194.
Mansfield, P., Pykett, I. L., Morris, P. G. & Coupland, R. E. 1978 *Br. J. Radiol.* **51**, 921–922.
Mansfield, P. & Pykett. I. L. 1978 *J. magn. Reson.* **29**, 355–373.
Mansfield, P., Morris, P. G., Ordidge, R. J., Coupland, R. E., Bishop, H. & Blamey, R. 1979 *Br. J. Radiol.* **52**, 242–243.
Mansfield, P. & Ordidge, R. J. 1980 (to be published).

PHILOSOPHICAL TRANSACTIONS OF THE ROYAL SOCIETY B BIOLOGICAL SCIENCES

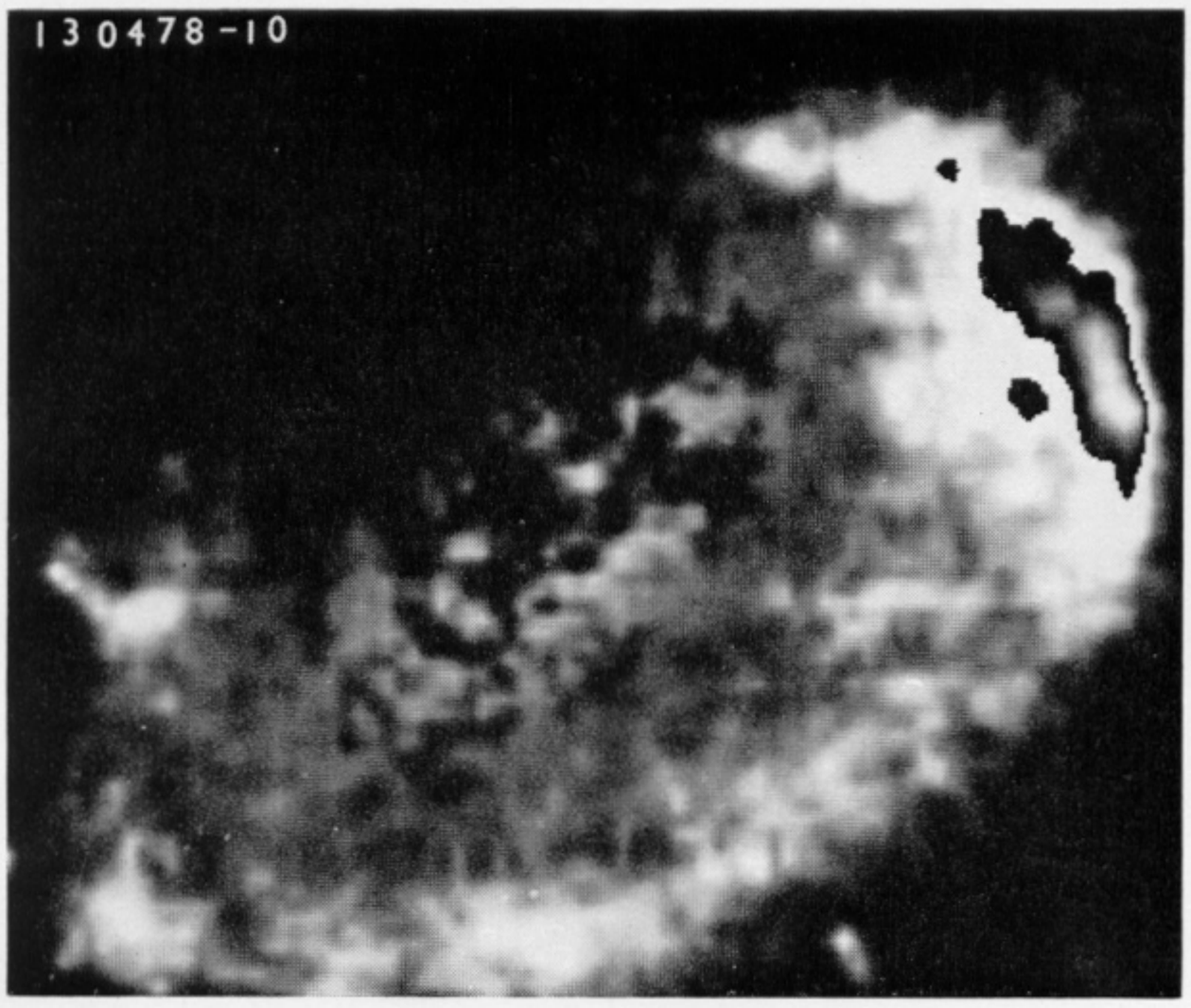

1

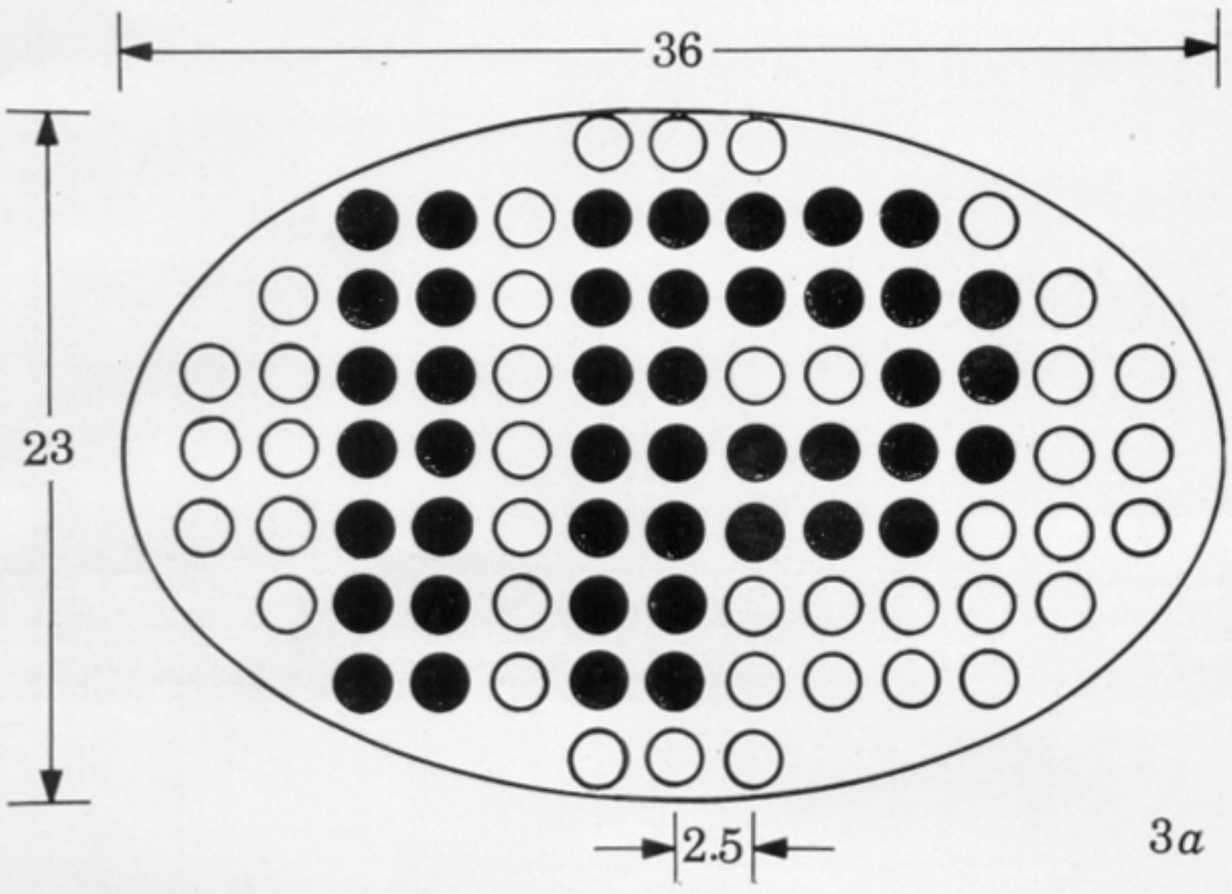

3a

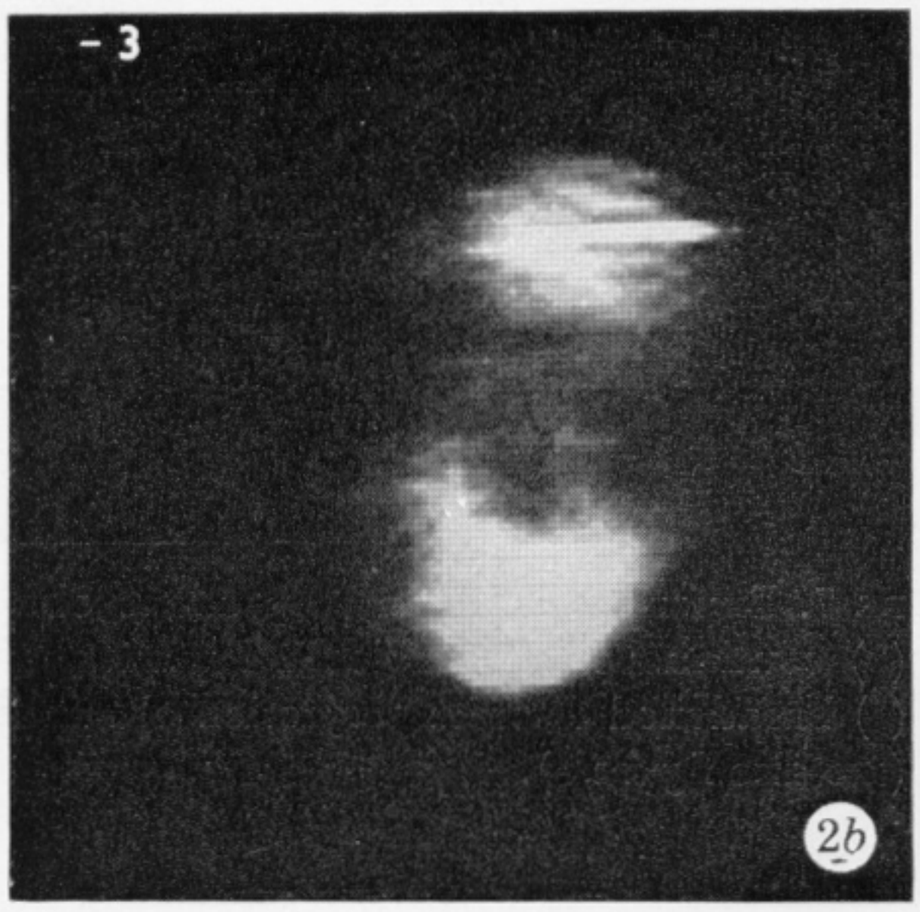

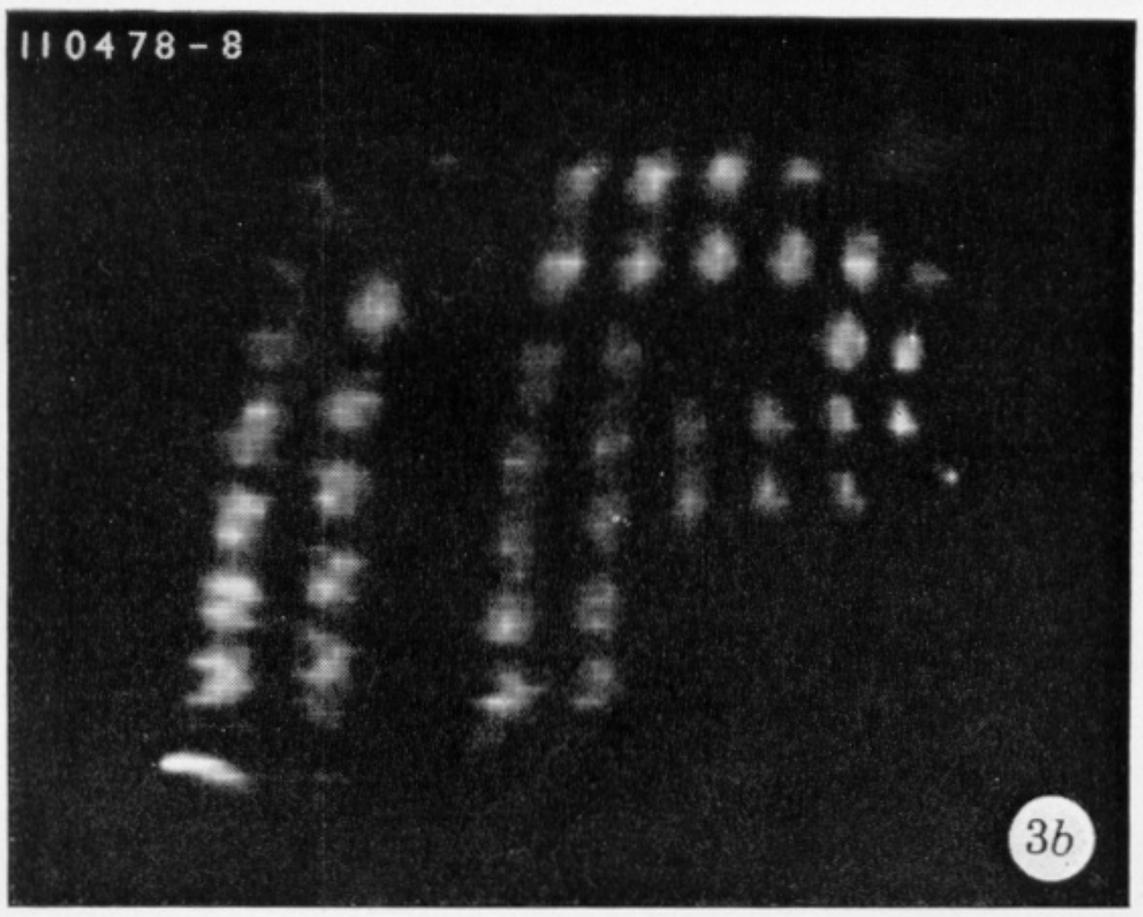

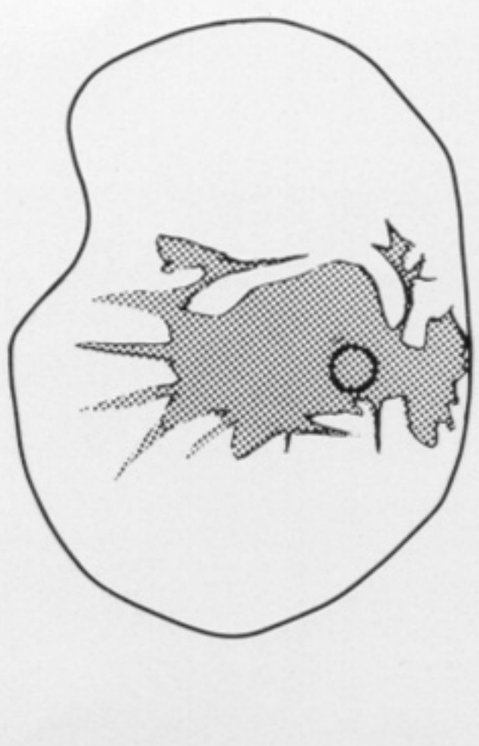

2c

FIGURE 1. Live cross-sectional image through the abdomen of P.M. at the L2–L3 level. Slice thickness is approximately 4.0 cm and the imaging time 40 min. See text and reference for further details.

FIGURE 2. Coronal projection scans through a tumorous breast shortly after mastectomy; (*a*) repetition period 0.3 s; (*b*) repetition period 0.15 s; (*c*) tracing taken from serial sections through the breast after n.m.r. scanning. This sketch shows the general outline of the breast with axillary tail uppermost. The shaded region shows the extent of the tumour which had its greatest depth and mass slightly left of the nipple (circle).

FIGURE 3. (*a*) Sketch of test phantom comprising an ellipical support matrix with an array of 19 mm diameter holes drilled with centres spaced at 25.4 mm intervals. (N.B. Dimensions in the diagram are shown in cm.) The filled circles represent test tubes containing water, forming the letters I P. (*b*) N.m.r. image of the phantom in (*a*) above. The slope and variation in intensity of the letters indicates the distortion of the gradient fields caused by non-uniformity of the main static magnetic field.

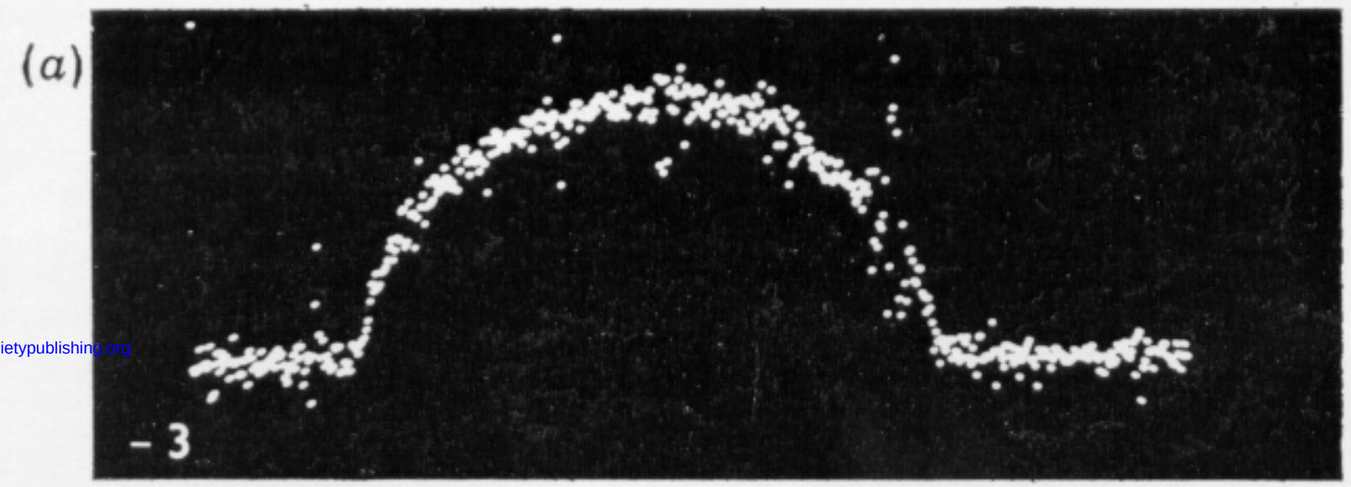

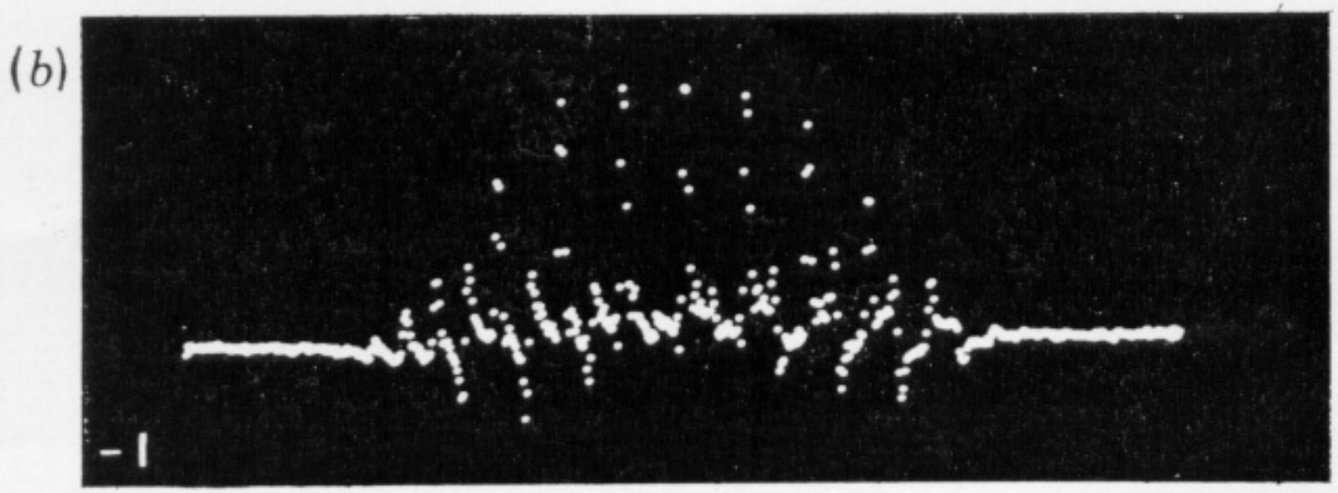

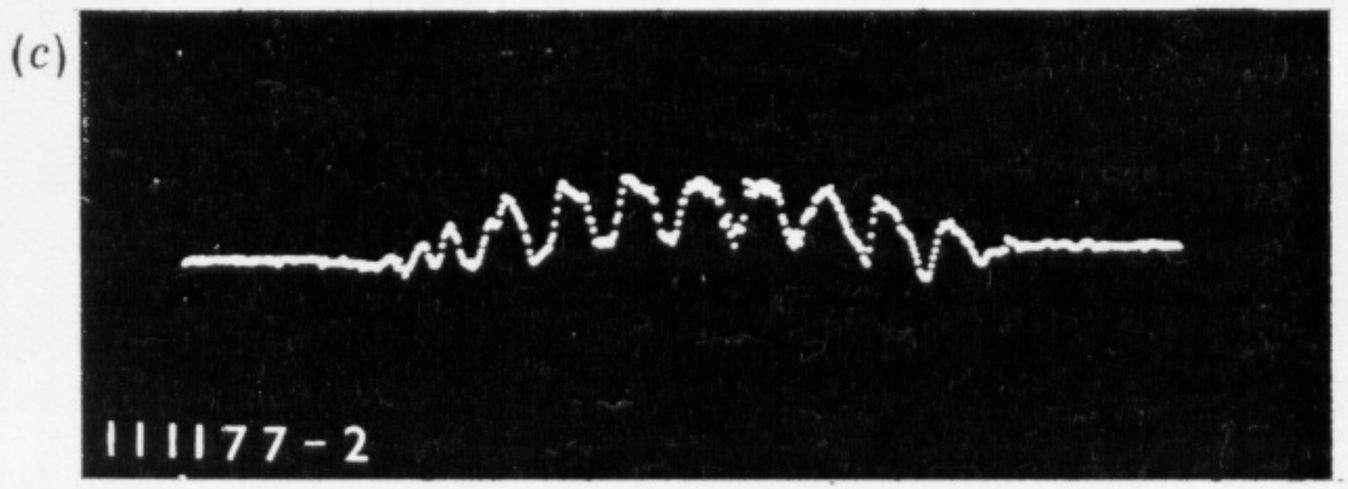

FIGURE 7. Experimental spin projections obtained at 15.0 MHz for a homogeneous cylinder of mineral oil: (*a*) continuous spin projection with steady gradient G_y; (*b*) discrete projection when G_y is modulated; (*c*) broadened discrete projection obtained as in (*b*) above, but with the addition of a steady gradient G_z (see also figure 5).

PHILOSOPHICAL TRANSACTIONS OF THE ROYAL SOCIETY B BIOLOGICAL SCIENCES

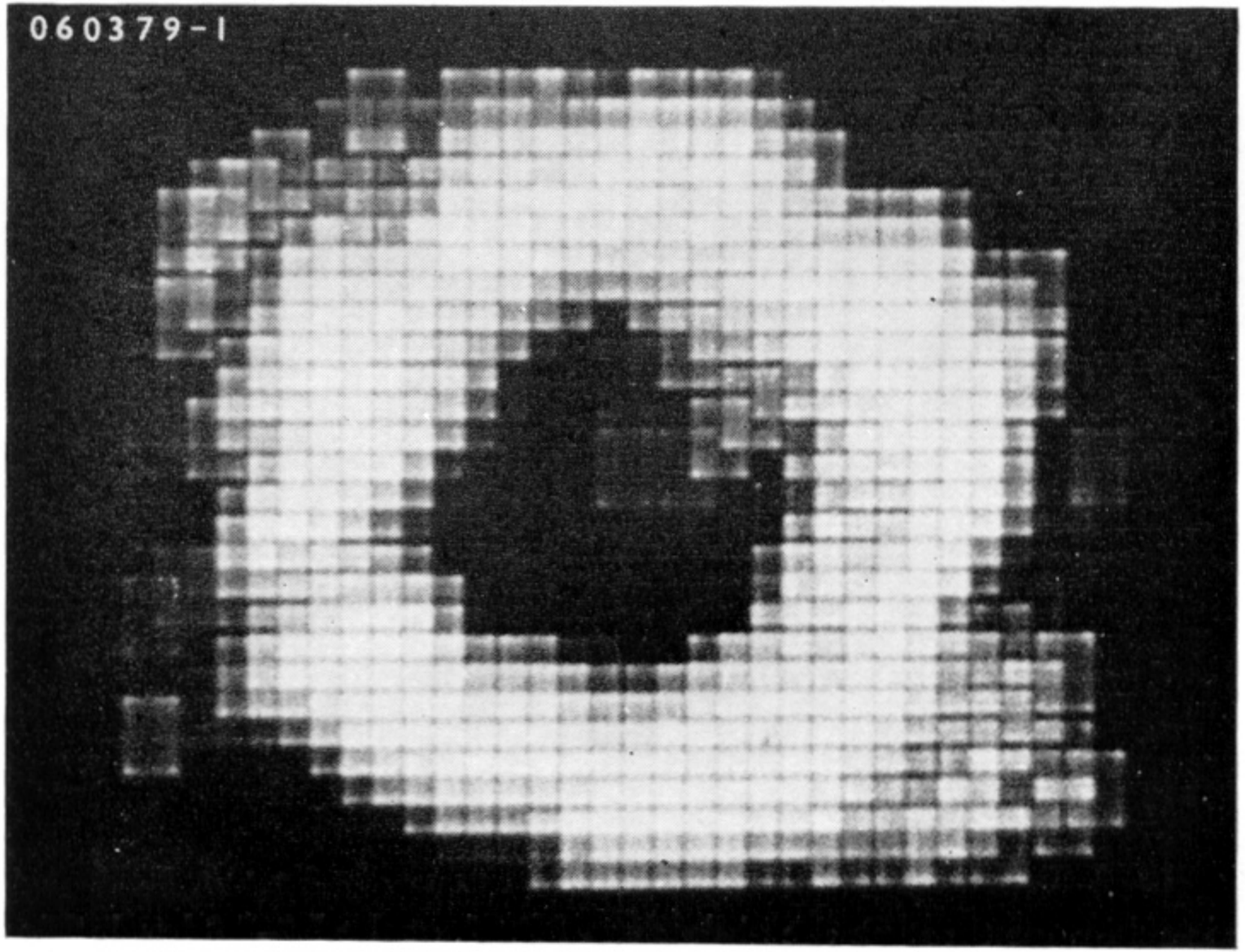

FIGURE 8. Echo planar image of a 1.5–2.0 cm thick selected slice through an extended cylindrical annulus of water, obtained at 4.0 MHz. The total image field is represented by a 32×32 array of original data points. This image was obtained in 8.0 s. The outer diameter of the phantom was 4.8 cm.

PHILOSOPHICAL TRANSACTIONS OF THE ROYAL SOCIETY B BIOLOGICAL SCIENCES